

Mass Loss Timescale of Star Clusters in External Tidal Field

Ataru TANIKAWA, and Toshiyuki FUKUSHIGE

*Department of General System Studies, College of Arts and Sciences,
University of Tokyo, 3-8-1 Komaba, Meguro-ku, Tokyo 153-8902*

tanikawa@provence.c.u-tokyo.ac.jp

(Received ; accepted)

Abstract

We investigate evolution of star clusters in external tidal field by means of N -body simulations. We followed seven sets of cluster models whose central concentration and strength of the tidal field are different. We found that the mass loss timescale due to escape of stars, t_{mloss} , and its dependence on the two-body relaxation timescale, $t_{\text{rh},i}$, are determined by the strength of the tidal field. The logarithmic slope [$\equiv d\ln(t_{\text{mloss}})/d\ln(t_{\text{rh},i})$] approaches to near unity for the cluster models in weaker tidal field. The timescale and the dependence are almost independent of the central concentration for clusters in the tidal field of the same strength. In our results, the scaling found by Baumgardt (2001) can be seen only in the cluster models with moderately strong tidal field.

Key words: celestial mechanics — star clusters — stellar dynamics

1. Introduction

The escape of stars from clusters is a long-standing problem in the study of dynamical evolution of star clusters. The theory for the escape was first developed by Ambartsumian (1938) and Spitzer (1940). It is based on the assumption that distant encounters between cluster stars will gradually set up a Maxwellian velocity distribution. Some stars have escape velocity of the cluster and they escape. The timescale that the distant encounters set up a Maxwellian velocity distribution corresponds to the two-body relaxation timescale (Chandrasekhar 1942, Spitzer 1987):

$$t_r = 0.065 \frac{v_m^3}{nm^2G^2 \ln \Lambda}, \quad (1)$$

where n is the number density of stars, m is the mass of the cluster stars, v_m is the average velocity of the stars, G is the gravitational constant, and Λ is the Coulomb logarithm. Every time the two-body relaxation time elapses, a cluster loses constant fraction of stars which have

escape velocity. Therefore, the mass loss timescale of a cluster is proportional to the two-body relaxation time.

This theoretical argument was confirmed by Baumgardt (2001) (hereafter, B01) in the absence of the external tidal field. He performed N -body simulations of evolution of star clusters, and showed that the mass loss of the cluster happened on the two-body relaxation timescale for energy cutoff clusters, and on the two-body relaxation with backscattering correction for radial (spatial) cutoff clusters.

However, the mass loss timescale from the clusters in external tidal field is remained unclear. The Collaborative Experiments (Heggie et al. 1998) demonstrated that the mass loss timescale does not scale with the two-body relaxation timescale, where multi-mass clusters moving in a steady tidal field were simulated. It turns out that the complication is due to the existence, at the initial setup, of population of stars that have energies above the escape energy and remain in a cluster before finding exits ("potential escapers"). Fukushige, Heggie (2000) (hereafter, FH) quantified the escape timescale of the potential escaper as a function of energy, and pointed out the escape timescale of the potential escaper is long enough to influence the whole mass loss timescale of clusters.

B01 performed N -body simulations of star clusters, where equal-mass clusters of $W_0 = 3$ King profiles (King 1966) evolve in the steady external tidal field. He investigated the dependence of mass loss timescale on two-body relaxation times using simulations whose particle numbers are $N = 128$ to 16384 . He found that the mass loss timescale of clusters, t_{mloss} , are proportional to, $t_{\text{rh}}^{3/4}$, the half-mass relaxation time to the power of $3/4$, where the half-mass relaxation time is given by

$$t_{\text{rh}} = 0.138 \frac{\sqrt{N} r_{\text{h}}^{3/2}}{\sqrt{m} \sqrt{G} \ln(\gamma N)}, \quad (2)$$

(Spitzer 1987) where N is the number of stars, r_{h} is the half-mass radius, and $\gamma = 0.11$ (Giersz, Heggie 1994). Baumgardt, Makino (2003) found almost the same scaling law for multi-mass clusters in time-dependent tidal field.

However, the $t_{\text{mloss}} \propto t_{\text{rh}}^{3/4}$ scaling is not convinced as an asymptotic behavior at larger N (or t_{rh}) for the following reason. In the limit of large N , the two-body relaxation timescale, t_{rh} , is much longer than the escape time delay, t_{e} , which is the duration from the moment when the star gets energy above the escape energy to that when it actually escapes from the cluster. Therefore, the mass loss timescale should be determined only by the half-mass relaxation time, i.e. $t_{\text{mloss}} \propto t_{\text{rh}}$.

The purpose of this paper is to investigate whether the $t_{\text{mloss}} \propto t_{\text{rh}}^{3/4}$ scaling obtained by B01 is an asymptotic behavior by means of N -body simulations. We perform sets of simulations of star clusters whose two-body relaxation timescale is larger than that of B01 and that are in the external tidal field with different strength.

The structure of the paper is as follows. We describe in detail the model of the cluster in

Table 1. Initial cluster models

Model name	W_0	$r_{t,i}$	$r_{t,i}/r_{kg}(W_0 = 3)$	$r_{t,i}/r_{kg}(W_0 = 7)$	N	$t_{dy,r=r_{t,i}}$
k3r0.8	3	2.50	0.80	0.36	128 – 131072	7.9
k3r1.0	3	3.13	1.0	0.44	128 – 131072	11
k3r1.3	3	4.20	1.3	0.60	128 – 32768	17
k3r2.2	3	6.98	2.2	1.0	128 – 32768	37
k3r4.5	3	14.0	4.5	2.0	128 – 16384	100
k7r1.0	7	3.13	1.0	0.44	128 – 131072	11
k7r2.2	7	6.98	2.2	1.0	128 – 32768	37

section 2. We show the results of N -body simulations in section 3. section 4 is for discussion. In section 5, we summarize this paper.

2. Simulation Method

We investigate the evolution of star clusters in the external tidal field by means of N -body simulations. We adopt the conventional model in which the cluster is assumed to move on a circular orbit in a spherically symmetric galaxy potential, taken to be that of a distant point mass M_g . We set the initial center of mass of the cluster at the origin $(x, y, z) = (0, 0, 0)$, with axes oriented so that the position of the galactic center is $(-R_g, 0, 0)$. We assume that the size of the globular cluster is much smaller than R_g . If the globular cluster rotates around the galactic center at an angular velocity $\Omega = (0, 0, \omega)$, the equation of motion of an individual cluster member can be expressed as

$$\frac{d^2\mathbf{r}_i}{dt^2} = -\nabla\Phi_{c,i} - 2\Omega \times \frac{d\mathbf{r}_i}{dt} + \omega^2(3x_i\hat{\mathbf{e}}_x - z_i\hat{\mathbf{e}}_z), \quad (3)$$

where \mathbf{r}_i is the position of the i -th particle, and $\hat{\mathbf{e}}_x$, $\hat{\mathbf{e}}_z$ are unit vectors that point along the x , z axes, respectively. The first term on the right-hand side in equation (3) is the gravitational acceleration from other particles in the cluster, the second term is the Coriolis acceleration, and the third term is a combination of the centrifugal and tidal forces. We used standard units (Heggie, Mathieu 1986), such that $M_i = G = -4E_c = 1$, where M_i is the initial total mass and E_c is the initial total energy within the cluster. In our simulations we used a softened gravitational potential expressed as

$$-\nabla\Phi_{c,i} = -\sum_{j=1, j \neq i}^N \frac{Gm_j(\mathbf{r}_i - \mathbf{r}_j)}{(|\mathbf{r}_i - \mathbf{r}_j|^2 + \varepsilon^2)^{3/2}}, \quad (4)$$

where m_j is mass of j -th particle and ε is a softening parameter. We set the softening parameter, ε , as $1/32$.

We used King's models (King 1966) to generate initial distribution of star clusters. We perform seven sets of simulations of star clusters whose initial dimensionless central potential,

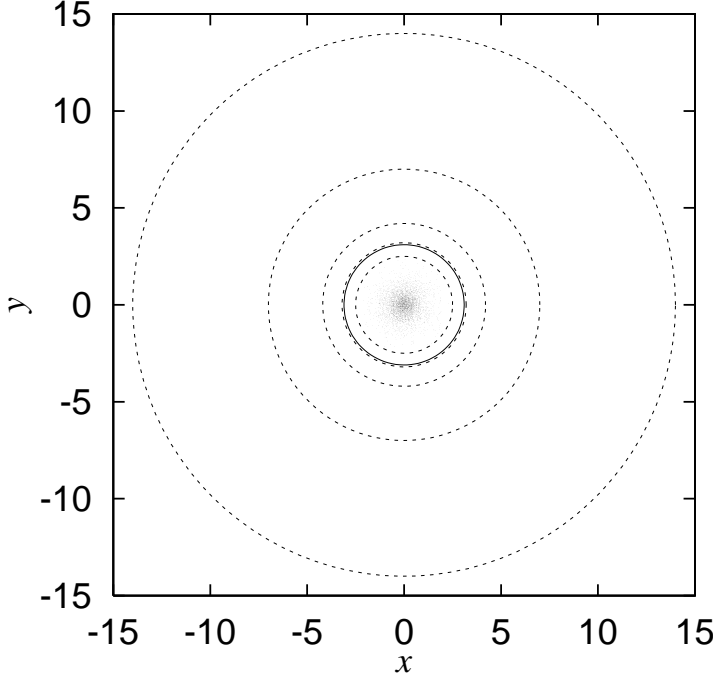


Fig. 1. Tidal radii, $r_{t,i}$, together with the particle distribution ($N = 4096$), for models with $W_0 = 3$ King model. The dashed circles show the tidal radii ($r_{t,i}$) determined by the external tidal field outward for models k3r0.8, k3r1.0, k3r1.3, k3r2.2 and k3r4.5, and the solid circle shows the King cutoff radius (r_{kg}) beyond which the density is zero in King model.

W_0 , of King model and initial tidal radii determined by the external field, $r_{t,i}$ are different, which are summarized in table 1. The number after "k" in model name indicates W_0 of King model. We set the strength of the external tidal field by giving the angular velocity ω in equation (4) using a relation, $\omega = \sqrt{GM_i/3r_{t,i}^3}$. The number after "r" in the model name indicates the tidal radius scaled by r_{kg} of $W_0 = 3$, where r_{kg} is the radius beyond which the density is zero in King model (hereafter, King cutoff radius). The values for r_{kg} in the standard unit are 3.13 and 6.98 for $W_0 = 3$ and 7, respectively. Figure 1 illustrates the tidal radii, $r_{t,i}$ for simulations of $W_0 = 3$ King model. The number of particles used for runs are listed in table 1. All particles have the same mass, $m = M_i/N$. We perform five runs whose realization of particle distribution are different for each N when $N \leq 8192$, and one run which $N \geq 16384$.

We perform numerical integrations of equation (3) using a leap-frog integration scheme with shared and constant timestep. The stepsize, Δt , is set to be as 1/64 in models k3r0.8, k3r1.0 and k7r1.0, and as 1/128 in models k3r1.3, k3r2.2, k3r4.5 and k7r2.2.

The force calculation is done with the Barnes-Hut algorithm (Barnes, Hut 1986) on GRAPE-5 (Kawai et al. 2000), a special-purpose computer designed to accelerate N -body simulations. Actually, we used the same code as in Fukushige, Suto (2001). We use only the dipole expansion and the opening parameter $\theta = 0.5$. It took about 500 CPU hours to complete

the most time-consuming run, $N = 32768$ of model k3r2.2 (about 7.2×10^6 timesteps). For smaller N simulations, the force calculation is done by direct summations (when $N \leq 4096$) and on host computer (without GRAPE-5, when $N \leq 512$).

Contrary to the standard star cluster simulations, our simulation uses the softened gravitational potential and the leap-flog integrator with relatively large stepsize. And also, the force calculation is done with the tree algorithm. These approaches are adopted in order to make the two-body relaxation timescale as large as possible. As will be discussed in the appendix, the approaches we adopted do not influence the results concerning on the escape from the cluster.

3. Results

3.1. Evolution of Total Mass

Figure 2 shows evolution of the total mass for all cluster models. The curves indicate the decrease in mass of the cluster defined by a tidal boundary. We define geometrically the cluster member as all stars within the tidal radius from the center of mass of the cluster. The tidal radius is expressed as

$$r_t = \left(\frac{GM}{3\omega^2} \right)^{1/3}, \quad (5)$$

where M is total mass of the members of the cluster at a given time. Since M depends on r_t itself, some iteration is usually required. We remove stars when they escape far enough (more than 4096 from the coordinate origin).

3.2. Mass Loss Timescale

Figure 3 shows the mass loss timescale, t_{mloss} , of clusters as a function of the initial half-mass relaxation time, $t_{\text{rh},i}$, for $W_0 = 3$ King cluster models. The mass loss timescale is here defined as the time when 50 % of the initial total mass is lost. Since we perform five runs when $N \leq 8192$, we adopt the means of these runs as the mass loss timescale, t_{mloss} . Table 2 shows the maximum deviations among these runs. The maximum deviation is defined as the largest difference from the mean. Since we use the potential softening and fix the softening parameters for all models, the initial half-mass relaxation time, $t_{\text{rh},i}$, is expressed as

$$t_{\text{rh},i} = 0.138 \frac{Nr_{\text{h},i}^{3/2}}{M_i^{1/2} G^{1/2} \ln(0.25r_{\text{h},i}/\varepsilon)}, \quad (6)$$

where $r_{\text{h},i}$ is the initial half-mass radius and $\varepsilon = 1/32$. Thus, the initial half-mass relaxation timescale, $t_{\text{rh},i}$, is estimated as $t_{\text{rh},i} = 470 \times (N/8192)$. The initial half-mass radii in the standard unit are $r_{\text{h},i} = 0.84$.

As can be seen from figure 3, a cluster in stronger tidal field lose its mass sooner. The difference of the mass loss timescale is considered to be due to the difference of the escape energy (the potential height at the Lagrangian point), which is lower for a cluster in stronger tidal field. Figure 4 shows change in energy of an individual star for k3r1.0 and k3r2.2 models

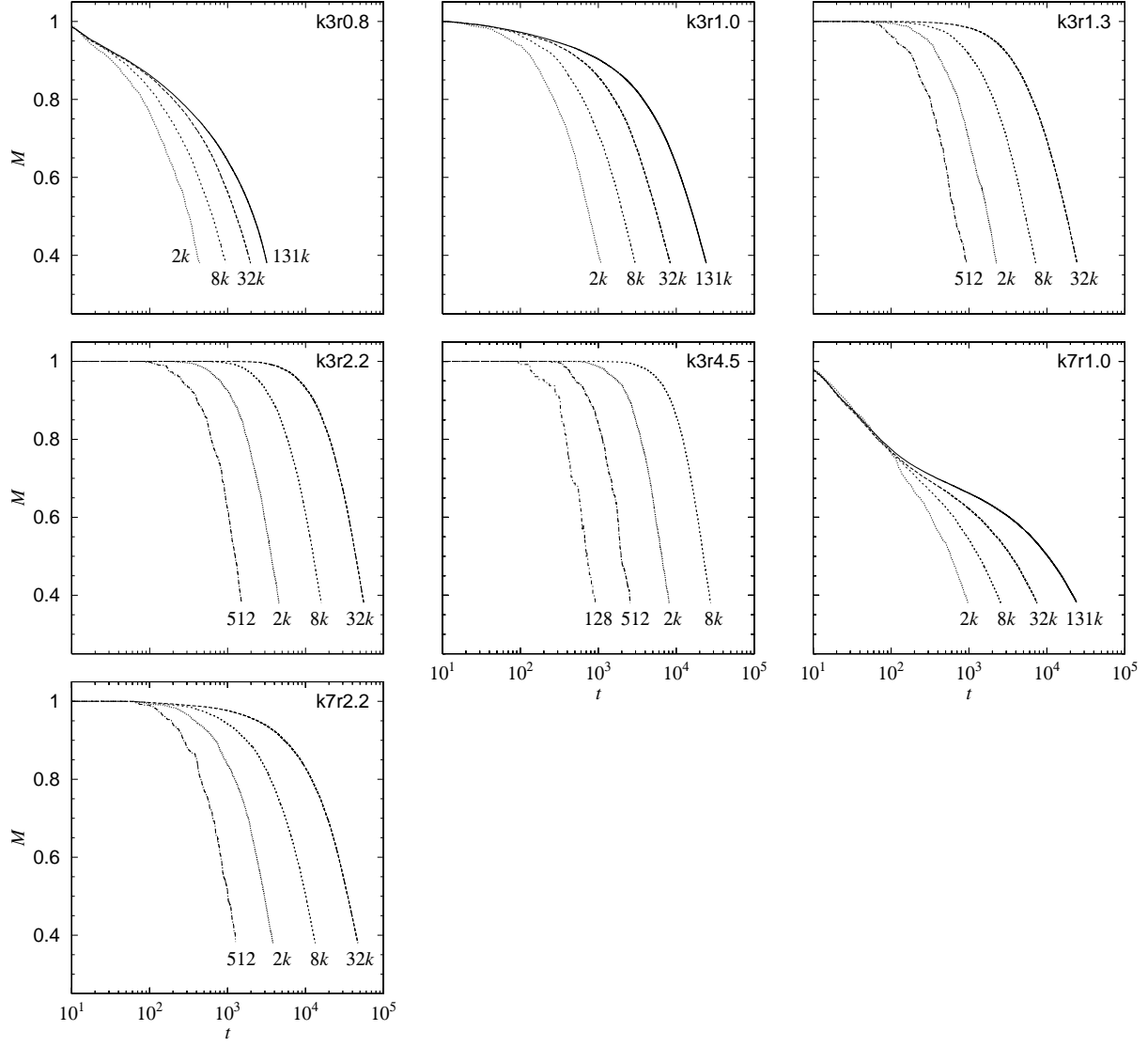


Fig. 2. Evolutions of the mass of the clusters. The numbers under the curves indicate the numbers of particles, N .

Table 2. Maximum deviation of t_{mloss} for $N \leq 8192$.

N	k3r0.8	k3r1.0	k3r1.3	k3r2.2	k3r4.5	k7r1.0	k7r2.2
128	11	32	62	40	86	41	151
256	21	20	41	65	145	33	94
512	22	19	40	90	129	48	53
1024	50	108	40	38	189	57	121
2048	37	40	115	230	138	36	123
4096	76	81	145	194	419	51	183
8192	92	166	201	118	286	200	211

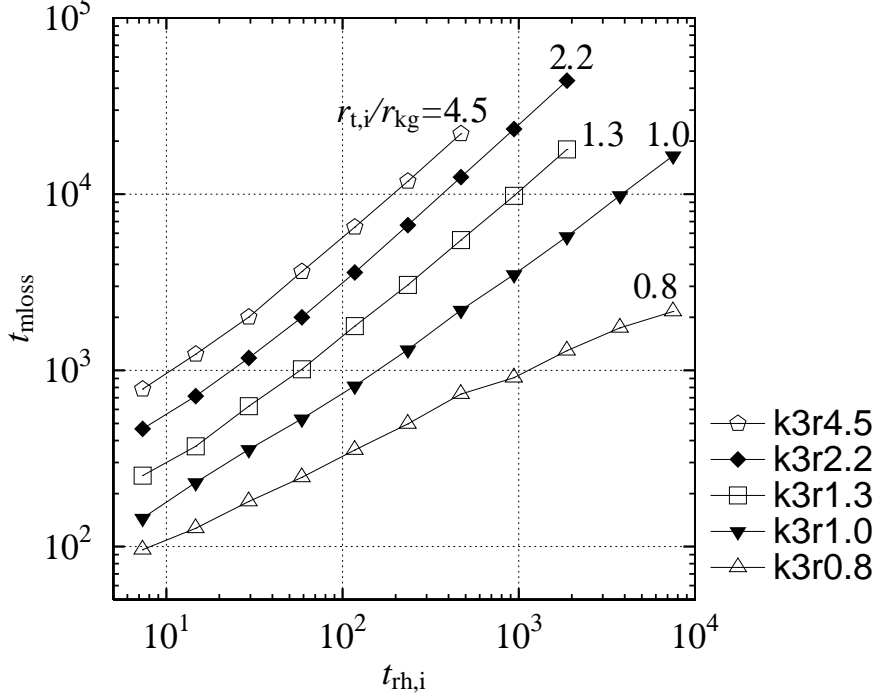


Fig. 3. Mass loss timescale of the clusters as a function of initial half-mass two-body relaxation timescale for $W_0 = 3$ King cluster models. The numbers near the curves indicate $r_{t,i}/r_{kg}$.

($N = 1024$). In figure 4 we plot $\{E_{\max,i}\}_{\text{med}}$, the median value of the maximum energy records at a given time, t_1 ;

$$E_{\max,i}(t_1) = \max_{t < t_1} \{E_i(t)\}, \quad (7)$$

$$E_i(t) = \frac{1}{2}(v_{xi}^2 + v_{yi}^2 + v_{zi}^2) + \Phi_{c,i} + \left(-\frac{3}{2}x_i^2 + \frac{1}{2}z_i^2\right) \quad (8)$$

of randomly selected 50 particles, where v_{xi} , v_{yi} , and v_{zi} are x, y, and z components of velocity of i -th particle, respectively. We do not update $E_{\max,i}(t_1)$ after stars escape from the cluster. The representative value, $\{E_{\max,i}\}_{\text{med}}$, may trace the energy acquired by two-body relaxations, on average. When stars obtain enough energy, they escape from cluster eventually. The dashed lines indicate the escape energy of each models, expressed as

$$E_{\text{crit}} = -\frac{3}{2} \frac{GM}{r_t}. \quad (9)$$

As shown in figure 4, the increase of $\{E_{\max,i}\}_{\text{med}}$ at $t < 600$ is very similar among models k3r1.0 and k3r2.2, which indicates that the relaxation processes in both models occur with almost the same timescale. However, because the escape energy in weaker tidal field is larger, it takes more time for a significant fraction of stars to escape in model k7r2.2 than in model k7r1.0.

Figure 5 shows logarithmic slopes, $\alpha(t_{\text{rh},i}) \equiv d \ln(t_{\text{mloss}}) / d \ln(t_{\text{rh},i})$, of the dependence on

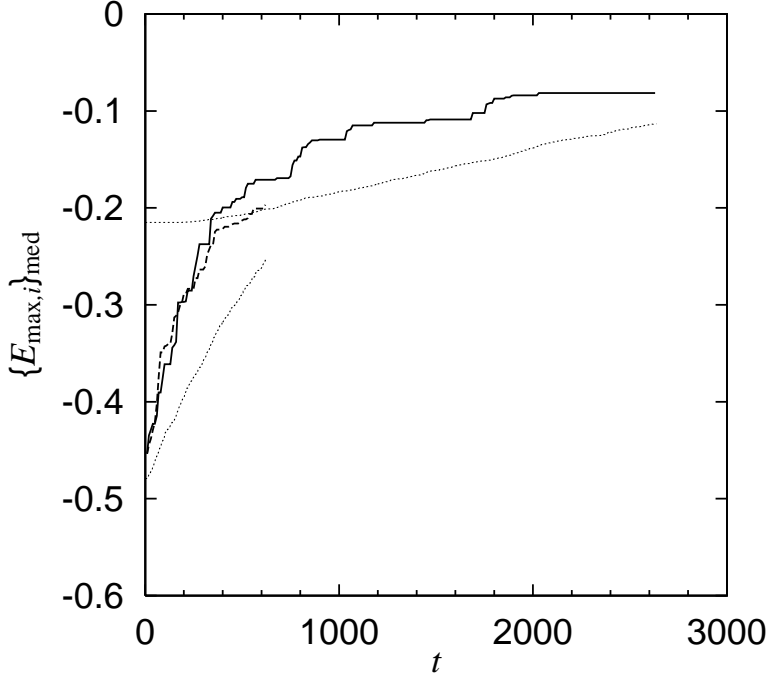


Fig. 4. Change in energy of an individual star for k3r1.0 and k3r2.2 models ($N = 1024$). The dashed and solid lines indicate $\{E_{\max,i}\}_{\text{med}}$ (the definition is in the text) in models k3r1.0 and k3r2.2, respectively. The upper dotted line indicates the escape energy in model k3r2.2 and the lower dotted line indicates that in model k3r1.0.

$t_{\text{rh},i}$ of the mass loss timescale shown in figure 3. Actually, we calculated the logarithmic slope $\alpha(t_{\text{rh},i})$ using a relation;

$$\alpha(t_{\text{rh},i}) = \frac{\log_{10}[t_{\text{mloss}}(t_{\text{rh},i})/t_{\text{mloss}}(t_{\text{rh},i}/2)]}{\log_{10}[t_{\text{rh},i}/(t_{\text{rh},i}/2)]}, \quad (10)$$

where $t_{\text{mloss}}(t_{\text{rh},i})$ is the mass loss timescale when the initial half-mass relaxation timescale is $t_{\text{rh},i}$.

As can be seen in figure 5, the logarithmic slope depends on the the strength of external tidal field. In model k3r1.0, where the initial distribution ($W_0 = 3$ King model) and the tidal field ($r_{t,i} = r_{\text{kg}}$) are set to be the same as in B01, we reproduce the asymptotic power, $\alpha(t_{\text{rh},i}) \sim 0.75$, obtained by him. Note that the initial half-mass relaxation timescale of the run with the largest N in B01 is about 230. On the other hands, when the tidal field is stronger (model k3r0.8) the slope is smaller [$\alpha(t_{\text{rh},i}) \sim 0.4$], and when it is weaker (models k3r1.3, k3r2.2, and k3r4.5) the slope is larger than $\alpha(t_{\text{rh},i}) = 0.75$. The slope $\alpha(t_{\text{rh},i})$ for the models in much weaker tidal field (more k3r2.2 and k3r4.5) seems to approach asymptotically $\alpha(t_{\text{rh},i}) \sim 0.9$, not 1.

The dependence of the slope is considered to be associated with the population of the potential escaper. For the clusters whose initial half-mass relaxation timescale is smaller (or smaller N), the escape time delay due to the potential escaper delays more the total mass loss

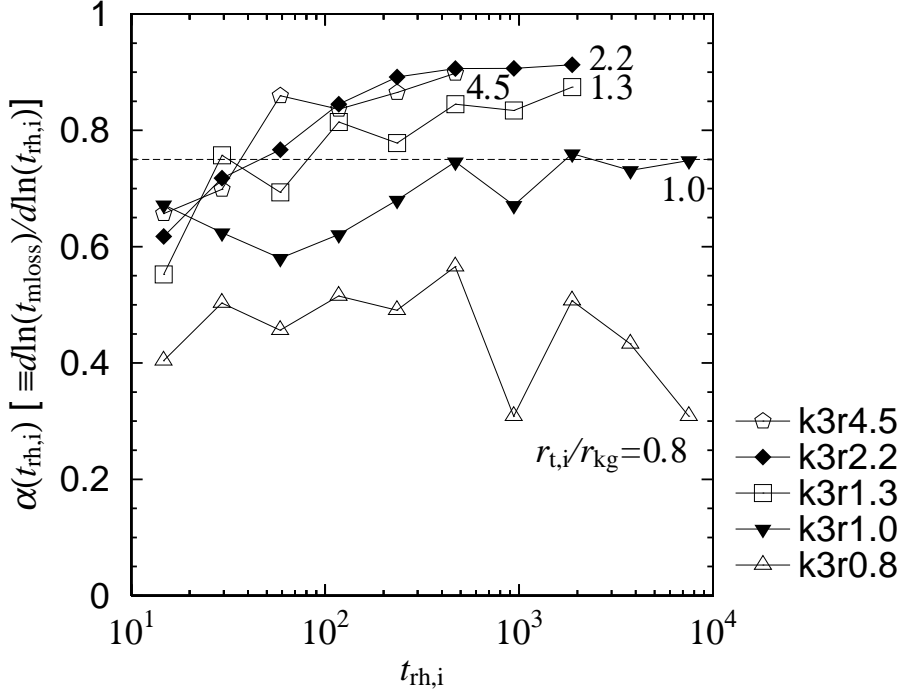


Fig. 5. Logarithmic slope $\alpha(t_{\text{rh},i})$ [$\equiv d \ln(t_{\text{mloss}}) / d \ln(t_{\text{rh},i})$] of dependence on the initial half-mass relaxation timescale. The dashed line indicates $\alpha(t_{\text{rh},i}) = 0.75$.

of clusters. Figure 6 shows the evolution of the fraction of potential escapers M_{pe}/M in the King $W_0 = 3$ cluster models ($N = 16384$, except for model k3r4.5, $N = 8192$). We can see that as the slope $\alpha(t_{\text{rh},i})$ shown in Figure 5 decreases, the fraction M_{pe}/M increases.

3.3. Effect of Initial Concentration

We investigate the dependence of the mass loss timescale on initial concentration of the cluster profile with $W_0 = 3$ and 7 King profiles. Figure 7 shows the mass loss timescale, t_{mloss} , as a function of the initial half-mass relaxation time, $t_{\text{rh},i}$, for models k3r1.0, k3r2.2, k7r1.0 and k7r2.2. In the models k7r1.0 and k7r2.2, the initial half-mass relaxation timescale is estimated as $t_{\text{rh},i} = 420 \times (N/8192)$. The initial half-mass radii in the standard unit are $r_{\text{h},i} = 0.77$, for $W_0 = 7$. As seen in figure 7, the differences between models k3r1.0 and k7r1.0 and between models k3r2.2 and k7r2.2 are small, which means the mass loss timescale does not depend so much on the concentration of the cluster. Figure 8 shows the logarithmic slope, $\alpha(t_{\text{rh},i})$ [$\equiv d \ln(t_{\text{mloss}}) / d \ln(t_{\text{rh},i})$].

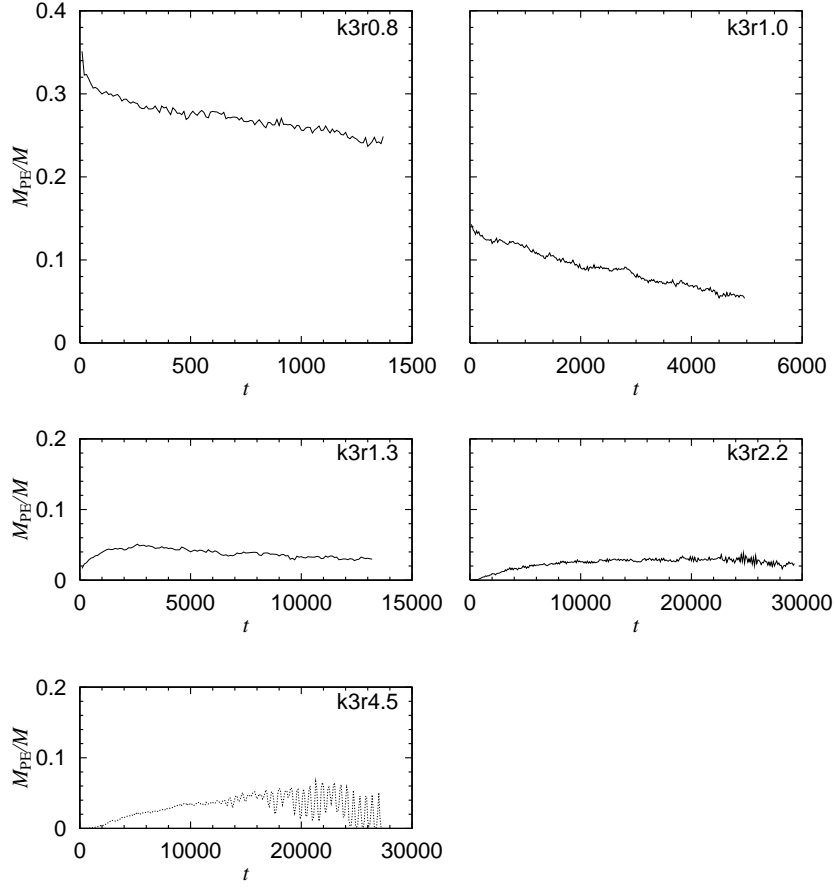


Fig. 6. Evolution of the fraction of the mass of potential escapers in the King $W_0 = 3$ clusters.

4. Discussion

4.1. Mass Loss Timescale for Small N

We discuss on the small $t_{\text{rh},i}$ (or small N) limit of the mass loss timescale, t_{mloss} , of clusters. When N is small, the half-mass relaxation time, $t_{\text{rh},i}$, is sufficiently small compared with the escape time delay, t_e , and it is expected to dominate the total mass loss timescale, t_{mloss} . In figure 9, we show the mass loss timescale of clusters scaled by the average dynamical time within the tidal radius, $t_{\text{dy},r=r_{\text{t},i}}$, which is expressed as

$$t_{\text{dy},r=r_{\text{t},i}} = \frac{2r_{\text{t},i}^{3/2}}{G^{1/2}M_i^{1/2}} \quad (11)$$

and listed in table 1, as a function of the initial half-mass relaxation timescale for $W_0 = 3$ King cluster models. The escape time delay is proportional to the average dynamical time (FH). In this figure, we don't plot that for model k3r4.5, since only this model with $N = 128$ and 256 experiences core collapse before the half mass is lost. As can be seen in figure 9, all of the scaled mass loss timescales, $t_{\text{rh},i}/t_{\text{dy},r=r_{\text{t},i}}$, approach to ~ 10 around $t_{\text{rh},i} \sim 7$, which means that

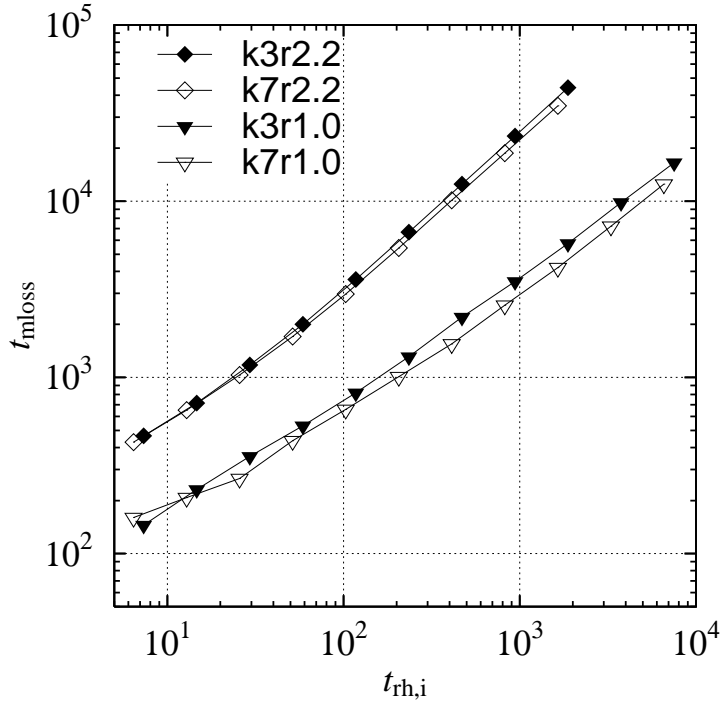


Fig. 7. Mass loss timescale as a function of the initial half-mass relaxation timescale for models k3r1.0, k3r2.2, k7r1.0 and k7r2.2.

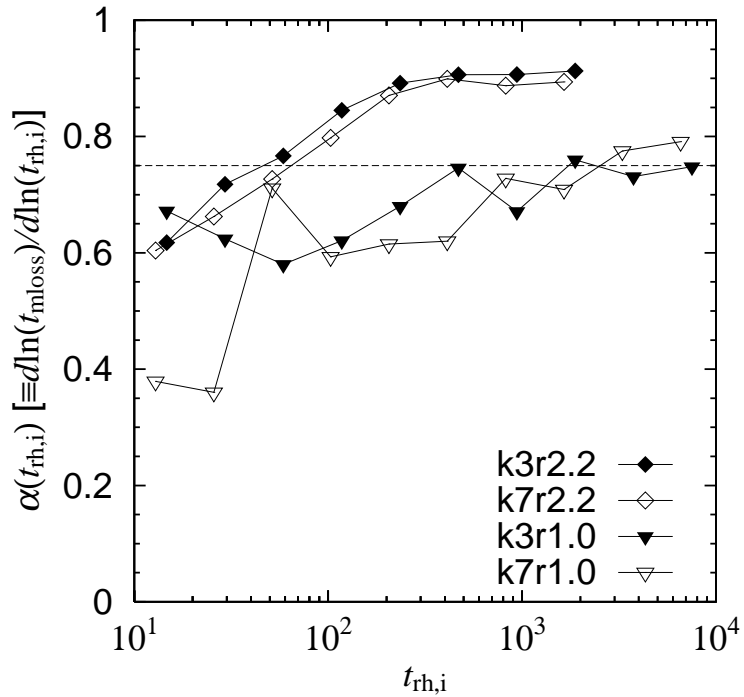


Fig. 8. Logarithmic slope $\alpha(t_{\text{rh},i}) [\equiv d\ln(t_{\text{mloss}})/d\ln(t_{\text{rh},i})]$ as a function of the initial half-mass relaxation timescale for models k3r1.0, k3r2.2, k7r1.0 and k7r2.2. The dashed line indicates $\alpha(t_{\text{rh},i}) = 0.75$.

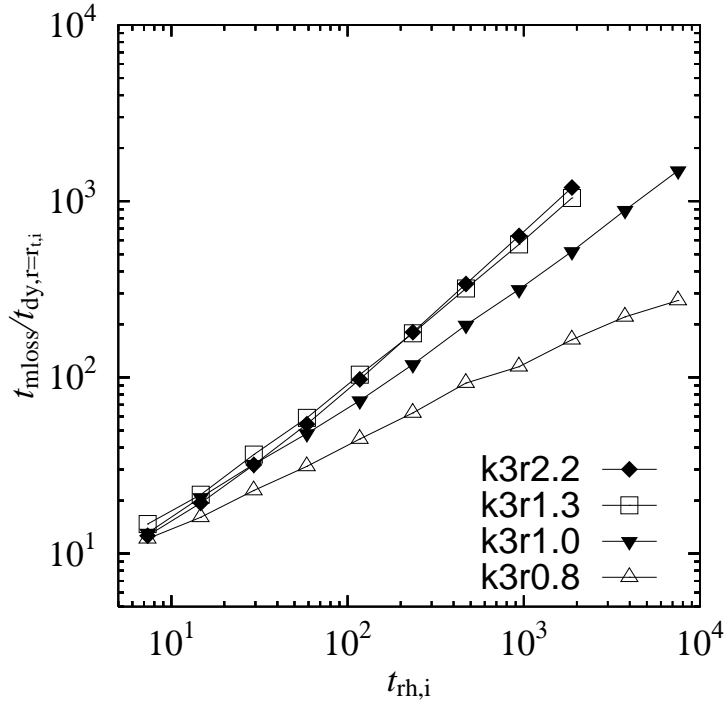


Fig. 9. Mass loss timescale scaled by the averaged dynamical time within the tidal radius as a function of the initial half-mass relaxation times for $W_0 = 3$ King cluster models.

the mass loss timescale is determined mainly by the averaged dynamical timescale or escape time delay in small $t_{\text{rh},i}$ (or small N) limit.

4.2. The Asymptotic Slope: $\alpha(t_{\text{rh},i}) \sim 0.9$

In section 1, we conjecture that the mass loss timescale should be determined only by the two-body relaxation timescale at its large limit. Our simulation results show that when the external tidal field is not strong (ex. model k3r2.2) the mass loss timescale is almost proportional to the half-mass relaxation timescale. However, its logarithmic slope seems to converge to slightly small value, $\alpha(t_{\text{rh},i}) \sim 0.9$. Here, we discuss origins of the small value 0.9.

One possible answer is that the two-body relaxation timescale we used may not correctly scale the real relaxation process occurred in the cluster. Another possible answer is that our simulation time span may be still not long enough to exclude the influence of the escape time delay on the mass loss timescale. Our simulation result and analytical estimate appear to favor the later possibility.

Figure 10 shows evolution of the Lagrangian radii as a function of time scaled by the initial half-mass relaxation time, $t_{\text{rh},i}$ for model k3r2.2 with $N = 1024, 2048, 4096$. We can see that the 20% Lagrangian radii of clusters with different N are in good agreement, which indicates that the half-mass relaxation time is surely a good measure of the internal relaxation process.

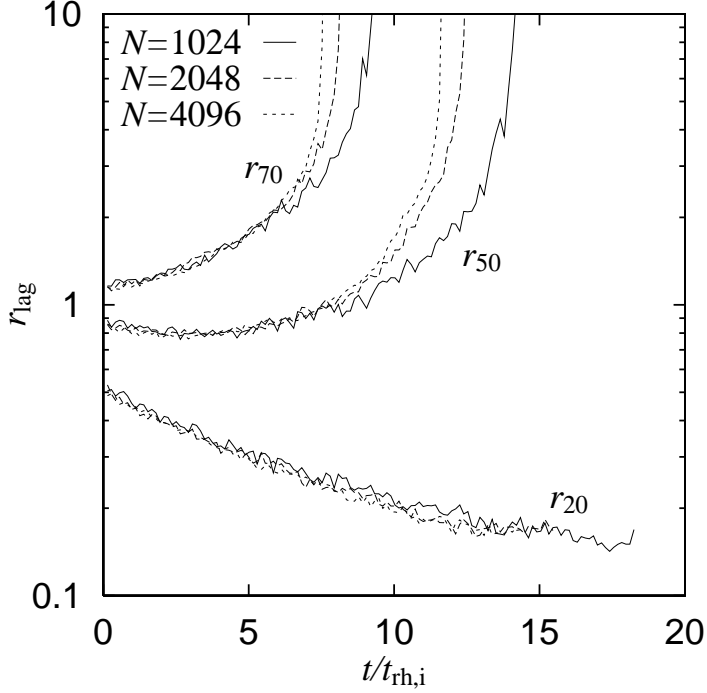


Fig. 10. Evolution of the Lagrangian radii containing 20, 50 and 70 % of the total mass as a function of time scaled by the initial half-mass relaxation time.

We estimate distribution of the escape time delay in model k7r2.2 using the results of FH, which gave the distribution of escape time delay for fixed King potential in $r_{t,i} = r_{kg}$ tidal field. According to this paper, the fraction of the initial potential escapers staying in a cluster, $P(t)$, is expressed by

$$P(t) = \sum_{\hat{E}} g_{\text{dis}}(\hat{E}) \left\{ \left[1 - f_{\text{non}}(\hat{E}) \right] (1 + 3.96\omega t \hat{E}^2)^{-0.729} + f_{\text{non}}(\hat{E}) \right\}, \quad (12)$$

where $\hat{E} = |(E - E_{\text{crit}})/E_{\text{crit}}|$ and E is the energy of a potential escaper, $g_{\text{dis}}(\hat{E})$ is the fraction of the initial potential escapers, and $f_{\text{non}}(\hat{E})$ is the fraction of non-escaper, which can not escape from the cluster due to the regular orbits, in the initial potential escapers. We took 0.04, 0.06, 0.08, 0.12, 0.16, and 0.24 as representative values of \hat{E} .

Figure 11 shows the distribution of escape time delay equation (12). In this figure we can see that at $t \sim 10^4$, which corresponds to the maximum of our simulation span, only half of the initial potential escapers have been depleted. This means that the mass loss timescale, t_{mloss} , of clusters are still affected not only by the initial half-mass relaxation time, $t_{\text{rh},i}$, but by the escape time delay, t_e within our simulation span. At least, 10 times simulation span may require to exclude the influence of the escape time delay.

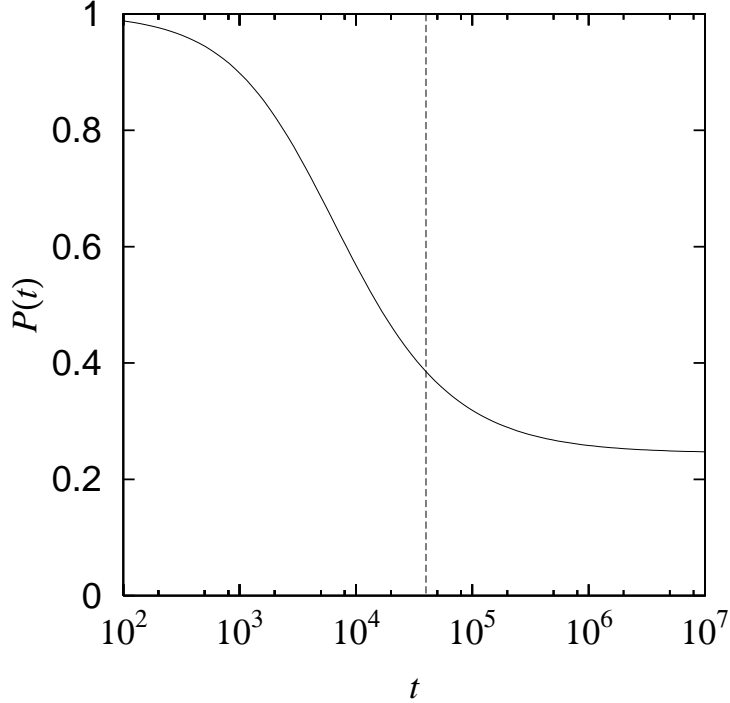


Fig. 11. Evolution of the fraction of the initial potential escapers based on the results of FH in the case of k7r2.2 series. Dashed line indicates $t = 40000$, which is equal to the largest simulation span.

5. Summary

We investigate the evolution of star clusters in external tidal field by means of N -body simulations. We follows evolution of seven sets of clusters, whose dimensionless central potential, W_0 , of clusters and the strength of external tidal field are different.

Our main conclusions are the following:

1. The mass loss timescale depends on the strength of external tidal field.
2. The Logarithmic slopes, $\alpha(t_{\text{rh},i})$ [$\equiv d \ln(t_{\text{mloss}}) / d \ln(t_{\text{rh},i})$], also depend on the strength of external tidal field. In model k3r1.0, whose run parameters are set to be the same as in B01, we can reproduce the asymptotic power, $\alpha(t_{\text{rh},i}) \sim 0.75$. However, when the tidal field is stronger (model k3r0.8) the slope is smaller [$\alpha(t_{\text{rh},i}) \sim 0.4$], and when it is weaker (models k3r1.3, k3r2.2, and k3r4.5) the slope is larger than $\alpha(t_{\text{rh},i}) = 0.75$. The slope $\alpha(t_{\text{rh},i})$ for the models in much weaker tidal field (more k3r2.2 and k3r4.5) is seen to approach asymptotically to near unity, but exactly $\alpha(t_{\text{rh},i}) \sim 0.9$.
3. The mass loss timescale is almost independent of the dimensionless central potential, W_0 .

We are grateful to Jun Makino and Holger Baumgardt for many helpful discussions. This research was partially supported by the Grants-in-Aid by the Japan Society for the Promotion of Science (14740127) and by the Ministry of Education, Science, Sports and Culture of Japan

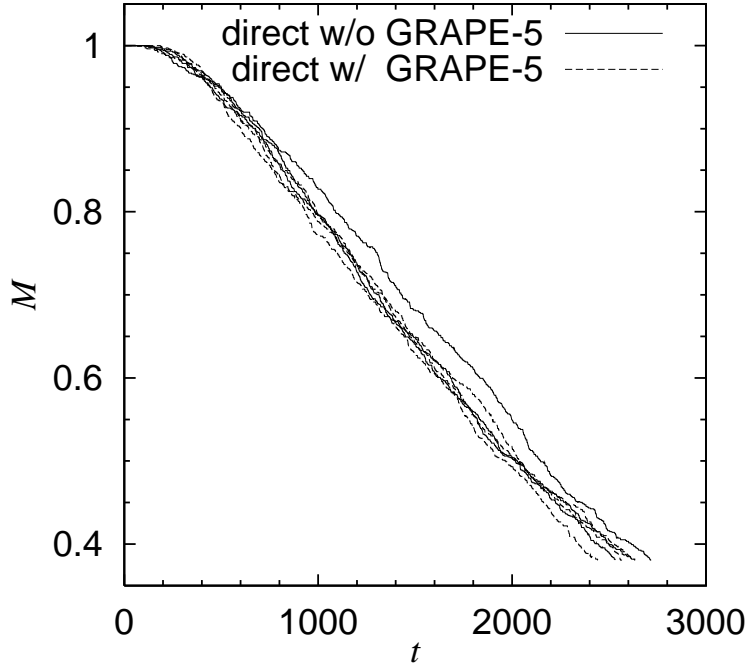


Fig. 12. Evolution of the total mass of cluster in model k3r2.2 ($N = 1024$). and solid lines are for runs with and without GRAPE-5, respectively.

(16684002).

Appendix 1. Reliability of Simulations

A.1.1. Force Accuracy

We use GRAPE-5 and the tree algorithm for the force calculations. Both arise artificial errors in the calculated force. When calculated with GRAPE-5 the force between two particles has a relative error of ~ 0.2 percent, because of the low accuracy of internal expressions in the GRAPE-5 chip (Makino, Ito, Ebisuzaki 1990, Kawai et al. 2000). The force calculation by the tree algorithm also contains error of similar magnitude, though it depends on the opening parameter. However, such errors caused by GRAPE-5 and the tree algorithm may not influence so much our results, because they are small compared to two-body relaxation effects (Hernquist, Makino, Hut 1993), which we want to handle correctly in our simulations. Figure 12 shows evolution of the total mass of clusters when force calculations are done by the direct summation with and without GRAPE-5, model k3r2.2 ($N = 1024$). The difference between runs with and without GRAPE-5 is smaller than its run-to-run variation. Figure 13 shows evolution of the total mass calculated using direct summation and the tree algorithm ($\theta = 0.5$) in model k3r2.2 ($N = 8192$). Both runs used GRAPE-5. The difference of the results is sufficiently smaller than its run-to-run variation.

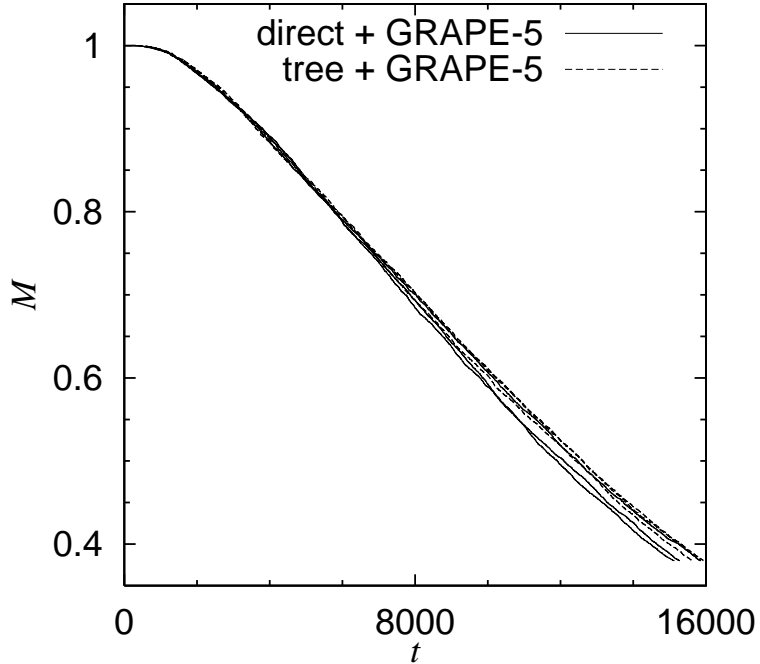


Fig. 13. Evolution of the total mass of clusters in model k3r2.2 ($N = 8192$). The solid and dashed lines indicates those obtained using direct summation and the tree algorithm, respectively. Three runs whose initial realization are different are performed for each case.

A.1.2. Accuracy of Time Integration

In our simulations, we use the leap-frog scheme, despite of the dependence of forces on the velocities. It is well-known that the nature of leap-frog scheme becomes worse in the presence of this dependence. However, figure 14 shows evolutions of the total mass of clusters when $\Delta t = 1/128$ and $1/256$ are converged, which means the leap-frog scheme with $\Delta t = 1/128$ does not influence our results.

A.1.3. Potential Softening

We use the potential softening for the force calculation. One might suspect if the two-body relaxation doesn't happen in such smoothed potential. Using the potential softening, close encounter between particles is surely suppressed. However, energy of particles is changed dominantly by accumulation of distant encounters, not by a few close encounters (Spitzer 1987). So, two-body relaxation should occur in the smoothed potential.

We check that the two-body relation happens with the softened potential. The upper panel of figure 15 shows the evolutions of the minimum potential in the clusters, Φ_{\min} , as a function of time scaled by the initial half-mass relaxation time, $t_{\text{rh},i}$, in the clusters of model k3r2.2 of $N = 1024, 2048, 4096, 8192$ and $\varepsilon = 1/32$. The central potential decreases owing to the two-body relaxation effect. As seen in the upper panel of figure 15, these curves are in good

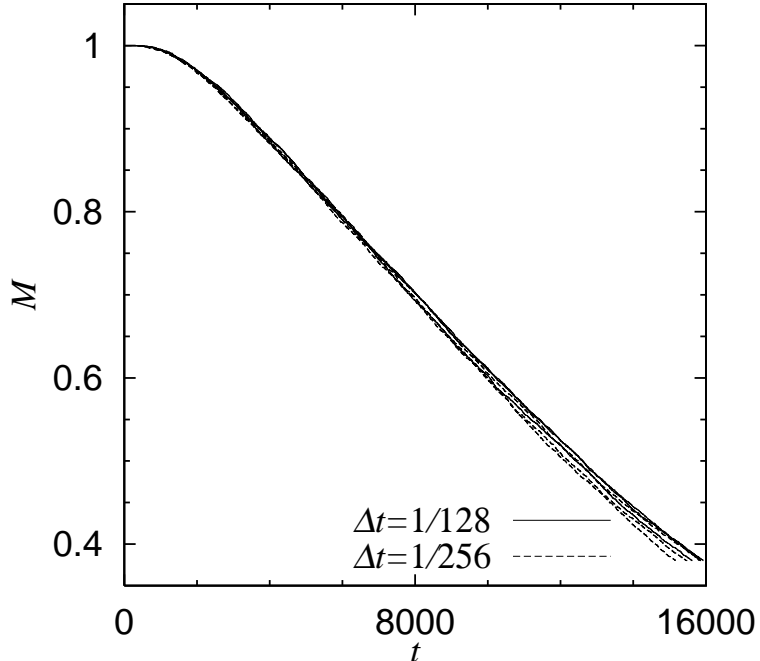


Fig. 14. Evolution of the total mass of clusters in model k3r2.2($N = 8192$). The solid and dashed lines indicates those obtained using timestep size $\Delta t = 1/128$ and $\Delta t = 1/256$, respectively. Three runs whose initial realization are different are performed for each case.

agreement and evolution of the central potential is scaled by the two-body relaxation timescale.

The lower panel of figure 15 shows the evolutions of Φ_{\min} in the clusters of model k3r2.2 of $N = 8192$ and $\varepsilon = 1/32, 1/48, 1/64$ as a function of timescale by the two-body relaxation timescale [equation (6)]. These curves are also in good agreement, which indicates that even with a softened potential, two-body relaxation occurs on the half-mass relaxation timescale, described by equation (6).

References

Ambartsumian, V. A., 1938, Ann. Leningrad State Univ., 22, 19
 Chandrasekhar, S., 1942, Principles of stellar dynamics (Chicago: The University of Chicago press)
 Barnes, J. E., & Hut, P. 1986, Nature, 324, 446
 Baumgardt, H., 2001, MNRAS, 325, 1323 (B01)
 Baumgardt, H., & Makino, J., 2003, MNRAS, 340, 227
 Fukushige, T., & Heggie, D. C., 2000, MNRAS, 318, 753 (FH)
 Fukushige, T., & Suto, Y., 2001, ApJ, 557, 11
 Giersz, M., & Heggie, D. C., 1994, MNRAS, 270, 298
 Heggie, D. C., Giersz, M., Spurzem, R., & Takahashi, K., 1998, in Highlights of Astronomy Vol. 11A, ed. J. Andersen (Dordrecht:Kluwer Academic Publishers), 591

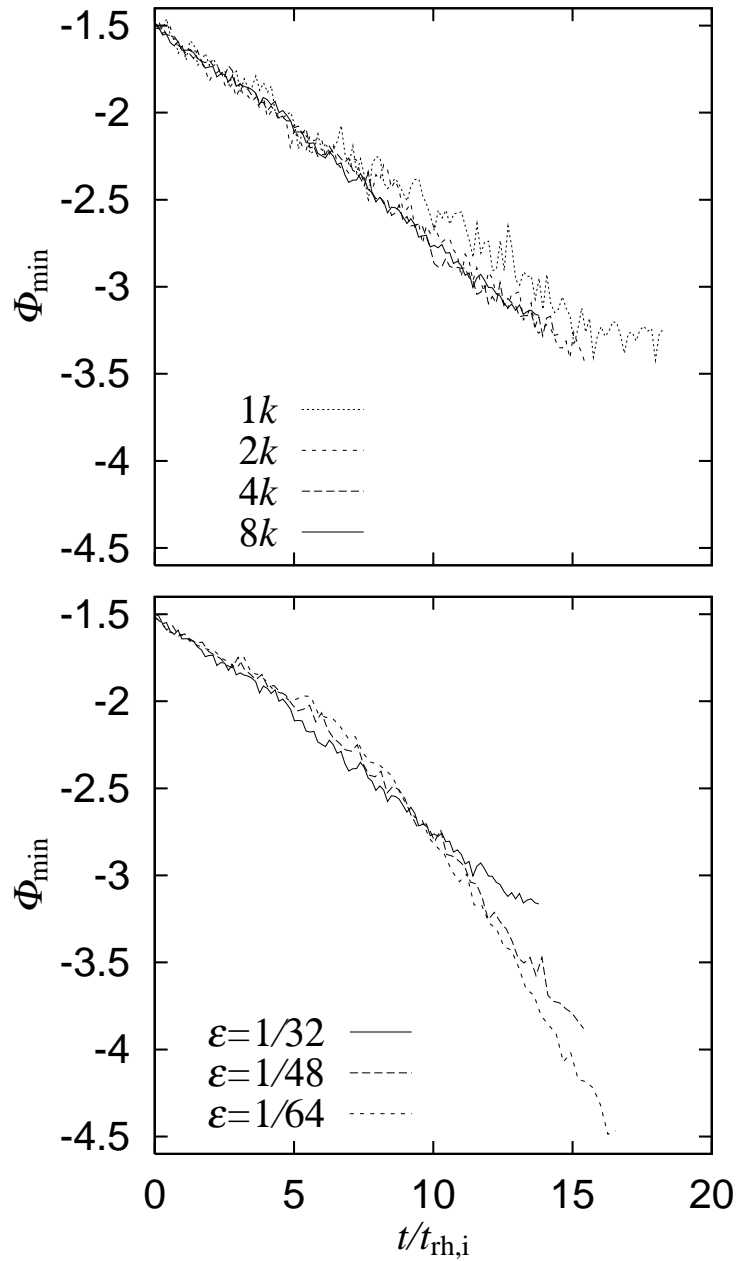


Fig. 15. Evolution of the minimum potential in clusters as a function of time scaled by the initial half-mass relaxation time in model k3r2.2 of $N = 1024, 2048, 4096, 8192$ and $\varepsilon = 1/32$ (top), and $N = 8192$ and $\varepsilon = 1/32, 1/48, 1/64$ (bottom).

Heggie, D. C., & Mathieu, R. D., 1986, in Lecture Notes in Physics Vol. 267, ed. P .Hut & S. McMillan (Berlin:Springer-Verlag), 233

Hernquist, L., Hut, P., & Makino, J., 1993, ApJ, 411, 53

Kawai, A., Fukushige, T., Makino, J., & Taiji, M., 2000, PASJ, 52, 659

King, I. R., 1966, AJ, 71, 64

Makino, J., Ito, T., & Ebisuzaki, T., 1990, PASJ, 42, 717

Spitzer, L., Jr., 1940, MNRAS, 100, 396

Spitzer, L., Jr., 1987, *Dynamical Evolution of Globular Clusters* (Princeton:Princeton University Press), ch.2